JOURNAL OF GUIDANCE, CONTROL, AND DYNAMICS
Vol. 20, No. 6, November–December 1997

Induced Oscillations of a Finite Plate

J. D. A. Walker,* C. N. Zhikharev,† and T. J. Delph‡
Lehigh University, Bethlehem, Pennsylvania 18015

Limit cycle oscillations are complex vibrations of airframe surfaces for which the cause-and-effect relationships are poorly understood. This fundamental investigation of oscillations of a finite two-dimensional flexible plate considers unforced vibrations, as well as situations where motion is induced by a convected vortex, a pressure wave, or an unsteady boundary-layer separation on the moving plate. It is found that very complex vibration patterns can occur and, with increasing nonlinearity, essentially chaotic motion can develop. When the plate is forced at frequencies close to the natural frequencies of the linear problem, a nonlinear resonance phenomenon occurs leading to a complex limit cycle behavior.

Nomenclature

a_i	= functional coefficients in normal mode expansion; Eq. (27)
D	= flexural rigidity
E	= Young's modulus
F	= Airy stress function
h	= plate thickness
$\bar{h}$	= scaled plate thickness; Eq. (16)
L	= plate length
M_{ij}	= integrals of normal mode derivatives; Eqs. (29–31)
N_x, N_y	= in-plane tensions
p	= dimensionless pressure difference
t	= dimensionless time
U	= uniform flow speed
u, v	= in-plane displacements
(x, y)	= Cartesian coordinates
Y	= scaled plate deflection; Eq. (22)
γ_i	= eigenvalues; Eq. (26)
ϵ	= coefficient of nonlinear term; Eqs. (15) and (21)
η	= scaled plate deflection, $\tilde{\eta}/\eta_m$; Eq. (12)
η_m	= representative plate deflection
θ	= normal scale; Eqs. (14) and (17)
ν	= Poisson ratio
ρ	= fluid density
ρ_p	= plate density
Φ_i	= eigenfunctions; Eq. (24)

I. Introduction

LIMIT cycle oscillations on airframe surfaces are known to be a continuing problem that can lead to excessive cabin noise, to stability problems, and in the worst cases, to structural failure.[1,2] The cause-and-effect relationships of this essentially nonlinear phenomenon are not well understood, and unfortunately, when such problems occur on aircraft, they are difficult (and expensive) to fix. The typical airframe environment in flight is rich in vortex motion, with vortices occurring naturally through viscous effects as a consequence of either certain three-dimensional geometrical configurations on the airframe[3] or boundary-layer separation from some upstream surface.

In general, vortices in motion impose a pressure field near a surface, which can act to deform and/or induce motion of a flexible panel; in addition, such fields contain moving zones of adverse pressure gradient, which can provoke separation in the viscous boundary layer on the surface. Here the term separation is used in the modern sense[4,5] to describe a catastrophic event wherein the boundary layer erupts and thereby abruptly leaves the surface. Such separation events may clearly be observed in various flows[3] at high Reynolds numbers; the process involves a rapidly moving thin plume of concentrated vorticity, and this makes the accurate calculation of such phenomena very difficult. In recent times, it has become possible to extend calculations partway into an unsteady separation event at high Reynolds numbers through the use of Lagrangian methods.[3–6] These calculations,[6] as well as recent experimental measurements,[3] show that unsteady separation of the boundary layer produces a sharp local spiky behavior in the pressure field near the surface; these pressure spikes can potentially have a significant effect in deforming the surface. In summary, the aeroelastic problem for a flexible surface bounding an external flow containing vortices generally involves a complex three-way mutual interaction between the external flow, the deforming surface, and the viscous boundary layer riding on the surface.

The present study is a first step toward developing an understanding of such interactions for incompressible flows containing vortices that pass over a flexible plate. The simplest configuration is a two-dimensional plate for which the deflection $w^* = w^*(x^*, t^*)$, with x^* measuring distance along the plate and t^* being time. Nonlinear oscillations of a plate in supersonic flow has previously been considered by Dowell,[7,8] who addressed the case of a simply supported or hinged plate; subsequent investigations[9–11] of simplified versions of this problem showed that chaotic motions of the supersonic panel problem were possible.

In the present study, the clamped two-dimensional plate will be considered; this is a configuration believed to be representative of typical aircraft panels, which are usually bonded to structural members of the airframe. In the following sections, a number of fundamental problems are considered to establish the nature of nonlinear vibrations in a subsonic flow. In all situations, the plate deflections are assumed sufficiently small so that the fluid motion above the plate is not affected to leading order; at the same time, the deflections are sufficiently large so as to be described by von Kármán plate theory.[8] First, the case of unforced vibrations is considered wherein an initial deflection is assumed and the subsequent vibration is studied. Second, the case of forced vibrations is addressed where the plate motion is induced by either a vortex convected over the plate or by a periodic pressure wave. In all cases, nonlinear effects lead to rather complex vibrations and, in some cases, to essentially chaotic plate motion. When the plate is forced at frequencies close to that of the natural (linear) plate frequencies, a complicated limit cycle behavior can occur in a phenomenon, which may be described as nonlinear resonance.

II. Governing Equations

The equations governing large deflections of a three-dimensional plate are well known[8,12]; they were originally derived[12] by Foppl but are now commonly referred to as the von Kármán plate equations.

Received Nov. 18, 1996; presented as Paper 97-0575 at the AIAA 35th Aerospace Sciences Meeting, Reno, NV, Jan. 6–9, 1997; revision received June 30, 1997; accepted for publication June 30, 1997.

*Professor, Department of Mechanical Engineering and Mechanics. Associate Fellow AIAA.
†Graduate Research Assistant, Department of Mechanical Engineering and Mechanics.
‡Professor, Department of Mechanical Engineering and Mechanics.

Let (x^*, y^*) be Cartesian coordinates measuring distance in the plate in the longitudinal and transverse directions, respectively, with corresponding in-plane displacements (u^*, v^*); denote the vertical deflection of the plate from equilibrium by w^*. For a two-dimensional plate such that variations in the y^* direction are negligible and for which $v^* \equiv 0$ and $u^* = u^*(x^*, t^*)$, $w^* = w^*(x^*, t^*)$, the plate equations reduce to

$$D\frac{\partial^4 w^*}{\partial x^{*4}} = \frac{\partial^2 F}{\partial y^{*2}}\frac{\partial^2 w^*}{\partial x^{*2}} - \rho_p h\frac{\partial w^*}{\partial t^*} - \left(p^* - p_0^*\right) \tag{1}$$

$$\frac{\partial^4 F}{\partial x^{*4}} + 2\frac{\partial^4 F}{\partial x^{*2}\partial y^{*2}} + \frac{\partial^4 F}{\partial y^{*4}} = 0 \tag{2}$$

Here F is the Airy stress potential function and D is the flexural rigidity defined by $D = h^3E/(1-\nu^2)$. In Eq. (1), p_0^* is the undisturbed pressure above and below the plate; p^* is taken to be a known function of x^*, t^*, which forces motion of the plate. Inasmuch as $w^* = w^*(x^*, t^*)$, it follows from Eq. (1) that the in-plane tension $N_x = \partial^2 F/\partial y^{*2} = N_x(x^*, t^*)$ and, consequently,

$$F = \tfrac{1}{2}N_x y^{*2} + A(x^*, t^*)y^* + B(x^*, t^*) \tag{3}$$

where A and B are arbitrary. It is easily shown that the strains reduce to

$$\varepsilon_x = \frac{\partial u^*}{\partial x^*} + \frac{1}{2}\left(\frac{\partial w^*}{\partial x^*}\right)^2, \qquad \varepsilon_y = \varepsilon_{xy} = 0 \tag{4}$$

where the in-plane tension and shear are given by

$$N_x = \frac{Eh}{(1-\nu^2)}\varepsilon_x, \qquad N_y = \nu N_x, \qquad N_{xy} = 0 \tag{5}$$

Substituting in Eq. (2) and the last two of Eqs. (5) and equating like coefficients of y to zero results in

$$\frac{\partial^4 N_x}{\partial x^{*4}} = \frac{\partial^2 N_x}{\partial x^{*2}} = \frac{\partial N_x}{\partial x^*} = 0 \tag{6}$$

with similar relations for A and B. It follows that $N_x = N_x(t^*)$ and from the first of Eqs. (5),

$$N_x(t^*) = \frac{Eh}{1-\nu^2}\left\{\frac{\partial u^*}{\partial x^*} + \frac{1}{2}\left(\frac{\partial w^*}{\partial x^*}\right)^2\right\} \tag{7}$$

Let the plate length be L and consider the situation where the plate is clamped at both ends with $u^*(0, t^*) = u^*(L, t^*) = 0$. Note that these conditions are commonly utilized in analysis of plate deflection problems, although Love[12] notes the difficulty of assuring that such conditions are actually satisfied in practical applications. Integration of Eq. (7) from 0 to L yields

$$N_x(t^*) = \frac{Eh}{2L(1-\nu^2)}\int_0^L \left(\frac{\partial w^*}{\partial x^*}\right)^2 \mathrm{d}x^* \tag{8}$$

and it follows that Eq. (1) reduces to

$$D\frac{\partial^4 w^*}{\partial x^{*4}} + \rho_p h\frac{\partial^2 w^*}{\partial t^{*2}} + p^* - p_0^* - \frac{Eh}{2L(1-\nu^2)}\left\{\int_0^L \left(\frac{\partial w^*}{\partial x^*}\right)^2 \mathrm{d}x^*\right\}\frac{\partial^2 w^*}{\partial x^{*2}} = 0 \tag{9}$$

with boundary conditions at $x^* = 0, L$ given by

$$w^* = \frac{\partial w^*}{\partial x^*} = 0 \tag{10}$$

For a given normal displacement, the longitudinal displacement u^* may be evaluated by integration of Eq. (7) from 0 to x^*.

It is noted in passing that Eq. (9) differs from that derived by Dowell[8] using geometrical arguments, by a factor of $(1-\nu^2)$ in the nonlinear term. However, a variety of conditions may be assumed in deriving the plate equation; for example, if it is assumed that $N_y = 0$ but $v^* \neq 0$, the same equation as obtained by Dowell[8] is found. The difference affects an $O(1)$ coefficient in Eq. (9) but has no influence on the results that follow.

III. Dimensionless Variables

In this study, plate motion induced by the flow is of principal interest, and the geometry is shown in Fig. 1. Let ρ be the fluid density and U be a typical fluid speed and define dimensionless variables in terms of ρ, U, and the plate length L according to

$$x = \frac{x^*}{L}, \qquad \tilde{t} = \frac{Ut^*}{L}, \qquad p = \frac{p^* - p_0^*}{\rho U^2} \tag{11}$$

and

$$\tilde{\eta} = w^*/\theta L, \qquad u = u^*/\theta^2 L \tag{12}$$

where θ is a dimensionless parameter whose form is to be determined; the plate deflections are taken to be small in the sense that $\theta \ll 1$. Substitution into Eq. (9) reveals that three independent dimensionless groups appear (in addition to θ), denoted by

$$\bar{E} = E/\rho U^2, \qquad \bar{h} = h/L, \qquad \bar{\rho}_p = \rho_p/\rho \tag{13}$$

and for the situations of interest here, it is anticipated that $\bar{E} \gg 1$, $\bar{h} \ll 1$, and $\bar{\rho}_p \gg 1$. The normal scale θ is determined by requiring that the forcing pressure term in Eq. (9) balance the bending moment, and this is the case if

$$\theta = \frac{12(1-\nu^2)}{\bar{E}\bar{h}^3} \tag{14}$$

The coefficient of the nonlinear term in Eq. (9) becomes

$$\tilde{\varepsilon} = \frac{12^3(1-\nu^2)^3}{2}\bar{E}^{-2}\bar{h}^{-8} \tag{15}$$

and it is evident that a distinguished limit problem exists for $\bar{E} \to \infty$ and $\bar{h} \to 0$ such that $\bar{h} = O(\bar{E}^{-1/4})$ and $\tilde{\varepsilon} = O(1)$. Formally defining

$$\bar{h} = 3^{\frac{3}{8}}2^{\frac{5}{8}}(1-\nu^2)^{\frac{3}{8}}\tilde{\varepsilon}^{-\frac{1}{8}}\bar{E}^{-\frac{1}{4}} \tag{16}$$

it follows from Eq. (14) that the normal scaling factor is

$$\theta = \left\{\frac{2}{3(1-\nu)^2}\right\}^{\frac{1}{8}}\tilde{\varepsilon}^{\frac{3}{8}}\bar{E}^{-\frac{1}{4}} \tag{17}$$

Consequently, in the parameter range of interest where nonlinear effects are significant, i.e., $\tilde{\varepsilon} = O(1)$, the plate deflections are $O(\bar{E}^{-1/4})$ and small in the limit $\bar{E} \to \infty$. When $\tilde{\varepsilon} \to 0$, a linear regime is obtained in which $\bar{h} \gg O(\bar{E}^{-1/4})$, i.e., a thicker plate, and the nonlinear term in Eq. (9) becomes progressively less significant.

The coefficient of the acceleration term in Eq. (9) is now

$$\bar{\rho}_p\bar{h}\theta = 3^{\frac{1}{4}}2^{\frac{3}{4}}(1-\nu^2)^{\frac{1}{4}}\bar{\rho}_p\tilde{\varepsilon}^{\frac{1}{4}}\bar{E}^{-\frac{1}{2}} \tag{18}$$

and is $O(1)$ for $\tilde{\varepsilon} = O(1)$ and $\bar{\rho}_p = O(E^{1/2})$. Consider some typical values for airflow past an aluminum plate at $U = 10$ m/s; here $E = 7 \times 10^{10}$ Pa, $\nu = 0.3$, $\rho = 1.2$ kg/m^3, $\rho_p = 2800$ kg/m^3, and it is readily confirmed that such values fit in the cited parameter range.

In subsequent sections, a number of vibration problems will be considered, both forced and unforced. The coefficient of the nonlinear term $\tilde{\varepsilon}$, defined in Eq. (15), depends principally on the physical

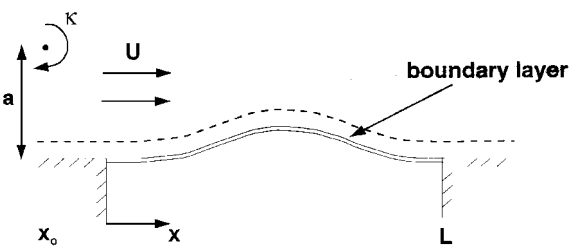

Fig. 1 Schematic of geometry.

properties of the fluid and the plate and does not reflect an influence associated with the deflection of the plate. Thus, a further scaling is introduced by $\eta = \tilde{\eta}/\eta_m$, where η_m is a value representative of the maximum displacement of the plate in a specific situation; a value of η_m will be specified for each subsequent problem considered. A scaled time is defined by $\tilde{t} = (\bar{\rho}_p \bar{h}\theta)^{1/2} t$, and the final form of the plate equation is

$$\frac{\partial^4 \eta}{\partial x^4} - \varepsilon \left\{ \int_0^1 \left(\frac{\partial \eta}{\partial x} \right)^2 \mathrm{d}x \right\} \frac{\partial^2 \eta}{\partial x^2} + \frac{\partial^2 \eta}{\partial t^2} + \frac{1}{\eta_m} p = 0 \tag{19}$$

which is to be solved subject to given initial conditions $\eta(x, 0)$ and $\dot{\eta}(x, 0)$ and the boundary conditions at $x = 0, 1$,

$$\eta = \frac{\partial \eta}{\partial x} = 0 \tag{20}$$

Here the overdot signifies a time derivative. The parameter ε is defined by

$$\varepsilon = \tilde{\varepsilon} \eta_m^2 \tag{21}$$

Finally, note that the plate deflection can be expressed in terms of the plate thickness by the relation

$$Y(x, t) = \frac{w^*}{h} = \frac{\varepsilon^{\frac{1}{2}} \eta}{\{6(1 - \nu^2)\}^{\frac{1}{2}}} \tag{22}$$

IV. Unforced Vibrations

In this section, the character of the vibrations will be considered when the forcing pressure is negligible and motion of the plate is induced by an initial displacement. When ε and p are zero, the general solution of Eq. (19) may be written in terms of the expansion

$$\eta(x, t) = \sum_{i=1}^{\infty} \left\{ A_i \cos \gamma_i^2 t + B_i \sin \gamma_i^2 t \right\} \Phi_i(x) \tag{23}$$

where $\Phi_i(x)$ are the eigenfunctions defined by

$$\Phi_i(x) = \cosh \gamma_i x - \cos \gamma_i x + Q_i (\sinh \gamma_i x - \sin \gamma_i x)$$
$$Q_i = \frac{\cosh \gamma_i - \cos \gamma_i}{\sinh \gamma_i - \sin \gamma_i} \tag{24}$$

and the eigenvalues γ_i satisfy

$$\cosh \gamma_i \cos \gamma_i = 1 \tag{25}$$

This relation has solutions for positive γ_i, which can easily be obtained numerically and which also may be represented in the expansion

$$\gamma_i = (2i + 1)(\pi/2) + (-1)^{i+1} b_0 - b_0^2 + \left\{ \tfrac{1}{3}(-1)^{3i} + 2(-1)^{i+1} \right\} b_0^3 + \cdots \tag{26}$$

where $b_0 = 1/\cosh\{(2i + 1)\pi/2\}$, for $i = 1, 2, 3, \ldots$. Note that the first eigenvalue $\gamma_1 = 4.7300$ (to five significant figures). The eigenvalues increase rapidly with increasing i, and consequently the frequencies represented in the normal mode expansion (23) are fairly high. The $\Phi_i(x)$ form a complete set of the normal eigenfunctions and the constants A_i and B_i can easily be determined for given initial conditions $\eta(x, 0)$ and $\dot{\eta}(x, 0)$.

Consider the nonlinear problem (19) with $p = 0$ and write the solution as

$$\eta(x, t) = \sum_{i=1}^{N} a_i(t) \Phi_i(x) \tag{27}$$

where the functional coefficients $a_i(t)$ are to be found and N is the number of terms retained in a series representation of the solution. In practice, N must be increased for a given vibration until there is no significant change in the solution. In the present study, calculations were carried out with up to 20 modes, but typically $N = 10$ was sufficient to assure good accuracy. Substitution of Eq. (27) into Eq. (19) leads to the equation set

$$\ddot{a}_i + \gamma_i^4 a_i = -\varepsilon \left\{ \sum_{j=1}^{N} \sum_{k=1}^{N} a_j(t) a_k(t) M_{jk} \right\} \sum_{\ell=1}^{N} a_\ell(t) M_{i\ell} \tag{28}$$

for $i = 1, 2, \ldots, N$ and

$$M_{ij} = \int_0^1 \Phi_i'(x) \Phi_j'(x) \, \mathrm{d}x \tag{29}$$

The eigenmodes $\Phi_i(x)$ are even about the midpoint of the plate at $x = \frac{1}{2}$ for $i = 1, 3, 5, \ldots$, and odd about $x = \frac{1}{2}$ for $i = 2, 4, \ldots$. It is evident, therefore, that $M_{ij} = 0$ for $i + j$ odd, and it can be shown that, for $i + j$ even,

$$M_{ij} = \frac{8 \gamma_i^2 \gamma_j^2}{\gamma_i^4 - \gamma_j^4} (B_j - B_i), \qquad B_j = (-1)^j \frac{\gamma_j \sin \gamma_j}{1 - (-1)^j \cos \gamma_j} \tag{30}$$

for $i \neq j$; in addition, the elements on the principal diagonal have values

$$M_{ii} = (-1)^i \gamma_i \frac{\left\{ \gamma_i \cos \gamma_i - 2 \sin \gamma_i + (-1)^i \gamma_i \right\}}{1 - (-1)^i \cos \gamma_i} \tag{31}$$

To study the nature of the plate response for various levels of nonlinearity, numerical solutions of Eq. (28) were obtained for different values of ε. Any set of initial conditions could be considered, but for simplicity the following were adopted:

$$a_i(0) = \delta_{i1}, \qquad \dot{a}_i(0) = 0 \qquad i = 1, 2, 3, \ldots \tag{32}$$

where δ_{ij} denotes the Kronecker delta. Thus, the first mode is excited with an initial amplitude $O(1)$; because the typical deflection is established by the initial condition, take $\eta_m = 1$ in Eq. (21).

The numerical method used is a combination of a fourth- and fifth-order Runge–Kutta method with automatic step size control as described by Press et al.[13] The specified initial time step was typically 10^{-4}, which was automatically adjusted as calculation progressed to ensure that the error at each step was 10^{-8} or less. Calculations were carried out in double precision and the single-step maximum error was also reduced to 10^{-10} as a check on the accuracy. The computed results presented are grid independent.

The linear case is obtained by taking $\varepsilon = 0$ in Eq. (28), and for this situation the plate vibrates with frequency γ_1^2 and the trajectory in the phase plane is an ellipse. A similar behavior was observed for small values of ε, but with increasing ε, a progressive increase in frequency occurs. The phase plane trajectories for the centerpoint of the plate for $\varepsilon = 1$ are shown in Fig. 2a in the time interval $t = 0, 5$; note that these and subsequent results are presented in terms of the dimensionless variable in Eq. (22). Only even modes ($i = 1, 3, 5, \ldots$) are excited by the initial condition (32) but if the initial condition contained odd modes ($i = 2, 4, \ldots$), the trajectories in Fig. 2a would not be altered because all such modes have zero deflection at $x = \frac{1}{2}$. A departure from a pure elliptic orbit may be seen in Fig. 2a, where the trajectories appear to meander in a narrow band. With increasing nonlinearity, the frequency of the oscillation increases and the vibration becomes more complex. The narrow band noted in Fig. 2a becomes much wider for $\varepsilon = 5$ in Fig. 2c. Because there is no physical mechanism for damping incorporated in Eq. (19), the maximum oscillation remains near the initial amplitude. On the other hand, comparison of the trajectories in Figs. 2a and 2c indicates that significantly higher velocities $\dot{Y}(0.5, t)$ are achieved with increasing nonlinearity. The trends noted continue with increasing nonlinearity, and results for a highly nonlinear case for $\varepsilon = 100$ are shown in Figs. 2d and 2e. The frequency of the vibration is substantially increased, and the phase plane trajectories are almost filled in toward the $\dot{Y}(0.5, t)$ axis, indicating a very complex and almost chaotic vibration pattern.

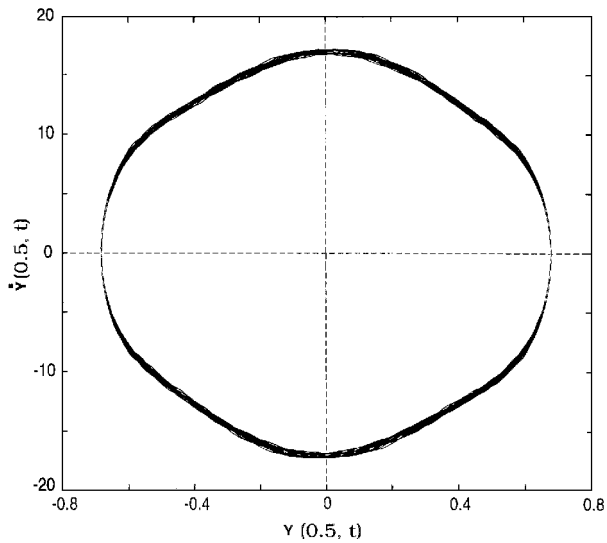

a) $\varepsilon = 1$

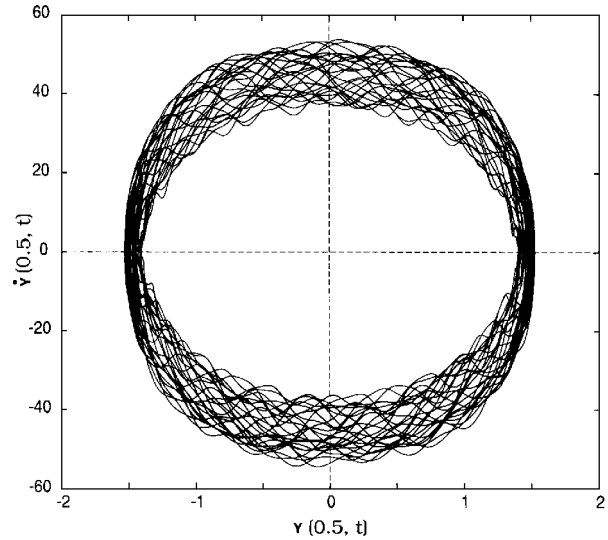

c) $\varepsilon = 5$

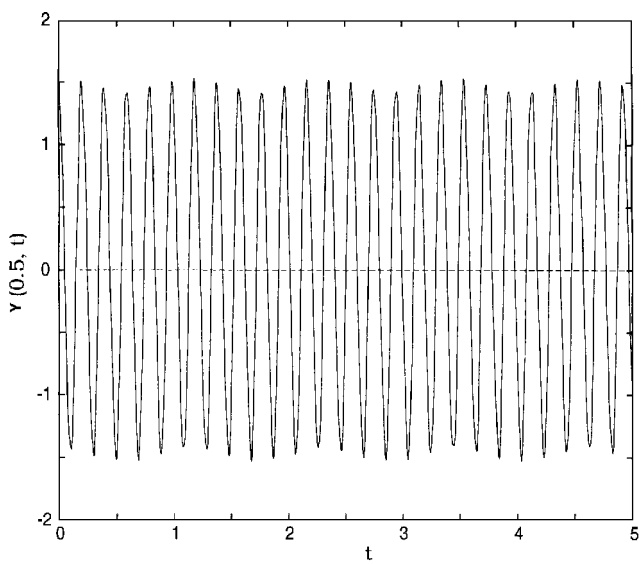

b) $\varepsilon = 5$

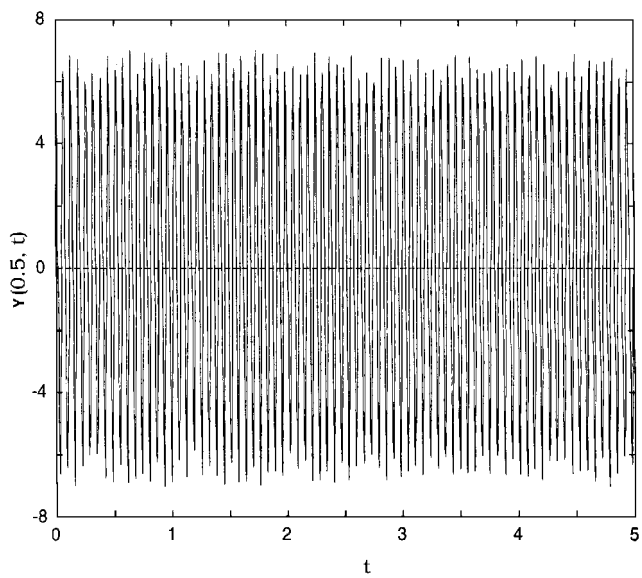

d) $\varepsilon = 100$

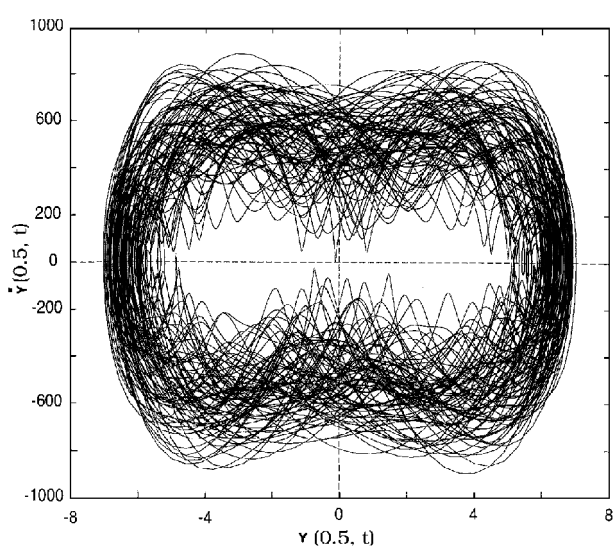

e) $\varepsilon = 100$

Fig. 2 Deflection of the center point of the plate $Y(0.5, t)$ vs time and phase plane trajectories for $t = 0, 5$.

Some insight as to how the vibration achieves the observed complexity with increasing nonlinearity can be obtained by carrying out a perturbation analysis for small ε. The appearance of a small parameter ε in Eq. (19) suggests the possibility of expanding the amplitude $\eta(x, \varepsilon, t)$ in a power series in ε. Assume simple initial conditions similar to Eq. (32), with $\eta_0(x, 0) = a_0\Phi_1(x)$, where a_0 is a known constant proportional to the maximum amplitude; a straightforward expansion soon leads to the appearance of secular terms, and it is necessary to introduce a slow time variable $\tau = \varepsilon t$. The expansion procedure has

$$\eta(x, \varepsilon, t) = \eta_0(x, t, \tau) + \varepsilon\eta_1(x, t, \tau) + O(\varepsilon^2) \tag{33}$$

and is well known[14]; consequently, the details of the calculation will be omitted here. The first term in the expansion is

$$\eta_0 = a_0\Phi_1(x)\cos\left\{\gamma_{11}^2 + \frac{3M_{11}^2a_0^2}{8\gamma_1^2}\varepsilon + \cdots\right\}t \tag{34}$$

Thus, even at the zeroth level, there is a shift to a higher frequency in the vibration of the first mode, whose value depends on the square of the initial amplitude, as well as ε. It may be readily shown that the first-order terms have the form

$$\eta_1(x, t, \tau) = \sum_{i=1}^{\infty} g_{1i}(t, \tau)\Phi_i(x) \tag{35}$$

and it can be shown that

$$g_{11}(t, \tau) = a_{11}(\tau)\cos\gamma_1^2 t + \frac{a_0^3M_{11}^2}{64\gamma_1^2}\cos\left\{3\gamma_1^2 + \frac{9M_{11}^2a_0^2}{8\gamma_1^2}\varepsilon + \cdots\right\}t \tag{36}$$

where $a_{11}(0) = -a_0^3M_{11}^2/(64\gamma_1^2)$ and $a_{11}(\tau)$ is to be determined such that secular terms in the expansion (33) are suppressed at second order. In addition, for $i \neq 1$

$$g_{1i}(t, \tau) = a_{1i}(\tau)\cos\gamma_i^2 t + \frac{a_0^3M_{11}M_{1i}}{4\left(9\gamma_1^2 - \gamma_i^2\right)}\cos\left\{3\gamma_1^2 + \frac{9M_{11}^2a_0^2}{8\gamma_1^2}\varepsilon + \cdots\right\}t + \frac{3M_{11}M_{1i}}{4\left(\gamma_1^2 - \gamma_i^2\right)}\cos\left\{\gamma_1^2 + \frac{3M_{11}^2a_0^2}{8\gamma_1^2}\varepsilon + \cdots\right\}t \tag{37}$$

Here $a_{1i}(0)$ is such that both $g_{1i}(0, 0) = 0$ and second-order secular terms are suppressed.

The expansion process can be carried out to higher order with increasing difficulty, but is not necessary because the trends are clear at this stage. It is evident from Eqs. (36) and (37) that the single leading-order mode has excited all even modes of vibration ($i = 1, 3, 5, \ldots$); in addition, near higher harmonics of the original mode have been produced, as well as modes with shifts to higher frequency. It may easily be confirmed that if the original displacement contained odd modes ($i = 2, 4, \ldots$), similar phenomena would occur for the odd modes. Consequently, an important effect of the nonlinearity (at least for small ε) is that a simple vibrational pattern rapidly becomes very complex, shifting to higher frequencies and multiple vibrational modes. This trend, which is reflected in Fig. 2, continues as ε increases to larger values until eventually the motion of the plate is essentially chaotic.

V. Vortex-Induced Vibrations

Now consider a situation where motion of the plate is forced by an external flow feature such as a convected vortex above the plate; this is common in aerodynamic flows and, as a representative case, a rectilinear vortex will be considered here. In general, the problem of pressure-induced vibrations differs from that of the preceding section; for example, as a model problem, consider the linear problem and suppose that suddenly at $t = 0$, the forcing pressure changes from zero to $P_0\Phi_1(x)$ above the plate, where P_0 is a constant amplitude. This event sets the plate in motion, and it is easily shown that

$$\tilde{\eta}(x, t) = \left(P_0/\gamma_1^4\right)\left(1 - \cos\gamma_1^2 t\right)\Phi_1(x) \tag{38}$$

implying an induced deflection $O(P_0/\gamma_1^4)$. Any pressure field can always be expressed at any time as a normal mode expansion, and because most will involve the leading eigenfunction $\Phi_1(x)$, the estimate of the typical induced deflection is useful. Therefore, in Eqs. (19) and (21), take $\eta_m = P_0/\gamma_1^4$; note that for $P_0 = O(1)$, η_m may actually be fairly small because $\gamma_1 = 4.73$.

For forced vibrations, the expansion (27) was used and the governing equations are the same as Eq. (28) but with $-P_i$ added to the right-hand side, where

$$P_i = \int_0^1 p(x, t)\Phi_i(x)\,\mathrm{d}x \tag{39}$$

To calculate a numerical solution, the integral (39) must be evaluated accurately at each time step. Because the integrand contains highly oscillatory terms for large i, the accurate evaluation of Eq. (39) is problematic with conventional methods, and instead a procedure due to Filon[15] was adopted. Let the interval (0, 1) be split into $M - 1$ equal parts of length h_1, and on the nth interval represent P as a linear function (for fixed t) according to $p = (p_{n+1} - p_n)x/h_1 + p_n$. The integrals in Eq. (39) may be evaluated analytically over the nth interval to obtain

$$\int_{x_n}^{x_{n+1}} p(x, t)\Phi_i(x)\,\mathrm{d}x = \frac{1}{\gamma_i}\{p_{n+1}Z_{i,n+1} - p_nZ_{i,n}\} - \frac{1}{h_1\gamma_i^2}\{S_{i,n+1} - S_{i,n}\} \tag{40}$$

where

$$S_{i,n} = \cosh\gamma_i x_n + \cos\gamma_i x_n - Q_i(\sinh\gamma_i x_n + \sin\gamma_i x_n) \tag{41}$$

and $Z_{i,n} = S'_{i,n}(x_n)/\gamma_i$ and Q_i is given by Eq. (24). The evaluation of Eq. (39) is accomplished by summing Eq. (40) over the interval from 0 to 1. A number of values of M were used as a check on the accuracy, and for the forcing functions considered here, values of M up to 5000 were found to give sufficient accuracy.

Now consider the case of a rectilinear vortex of strength κ, which is located at a distance a above the plate and is convected to the right in a uniform flow of speed U with convection velocity V_c as shown in Fig. 1. Let $V_c = \alpha U$, where α is defined as the fractional convection rate; it is easily shown[16] that $\alpha = 1 - \kappa/(2aU)$. In terms of the variables defined in Sec. III, the pressure field is given by

$$p(x, t) = \frac{4P_0\beta^2}{\bar{x}^2 + \beta^2}\left\{1 - \frac{2\beta^2}{\bar{x}^2 + \beta^2}\right\} \tag{42}$$

where $P_0 = (1 - \alpha)^2$, $\beta = a/L$ is an aspect ratio, and

$$\bar{x} = x - x_0 - \tilde{\alpha}t$$

Here $\tilde{\alpha} = \alpha(\tilde{\rho_p}\tilde{h}\theta)^{1/2}$ is a modified convection rate, and the vortex is located at $x = x_0$ at $t = 0$. The typical deflection parameter is taken as $\eta_m = P_0/\gamma_1^4$ in Eq. (19).

Calculations were carried out for a number of $O(1)$ values of $\tilde{\alpha}$ and β, and it was found that these parameters do not have a significant influence on the results. The representative calculations reported here are for $\beta = \frac{1}{2}$ and $\tilde{\alpha} = 1$. The plate was assumed to be at rest at $t = 0$, and the vortex was then inserted abruptly into the flow at $x = x_0$. The physical situation envisaged here is where a vortex is created abruptly via a separation from some upstream surface; in this process the plate responds to the influence of the vortex instantly at $t = 0$ and starts to vibrate.

The parameter x_0 has a major influence on the nature of the vibration. Consider, first, the case where the vortex is introduced at $x_0 = -0.5$, i.e., one-half a plate length upstream of the leading-edge

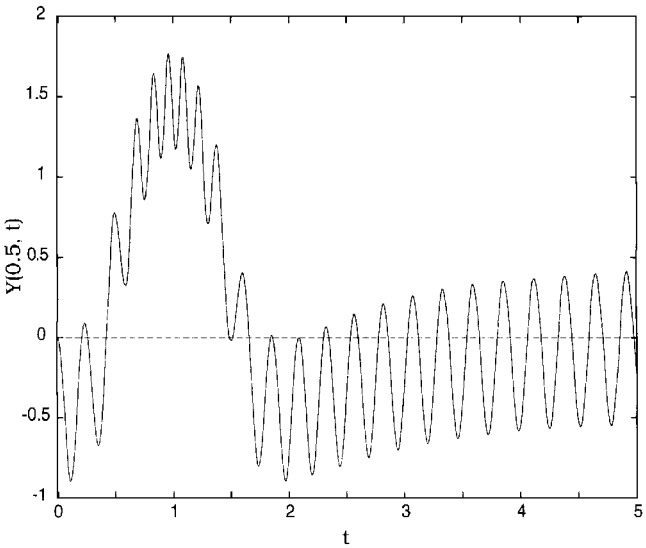

a) $\varepsilon = 5$

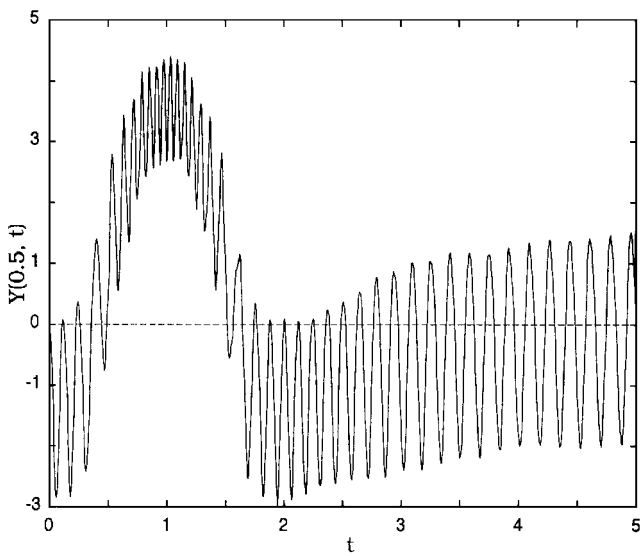

b) $\varepsilon = 500$

Fig. 3 Centerpoint deflection for $x_0 = -0.5$.

of the plate. As shown in Fig. 3, upon insertion of the vortex, the plate starts to vibrate immediately as it feels the pressure field of the vortex. As the vortex approaches and passes over the plate, the plate is drawn outward toward the vortex while oscillations associated with the initial insertion continue. As the vortex center passes over the trailing edge of the plate at $t = 1.5$, the mean deflection becomes negative and ultimately approaches zero as the vortex moves farther away from the plate. For smaller values of ε, the frequency of the oscillations is relatively low, but as shown in Fig. 3 for $\varepsilon = 5$ and 500, the frequency increases with increasing nonlinearity. As shown in Fig. 3b for $\varepsilon = 500$, the induced oscillations have increased in amplitude and frequency; they have become complex but still remain fairly regular. Note that if the vortex is started far upstream, the background oscillations are, in general, rather small because the pressure pulse due to the insertion of the vortex is then small at the plate itself.

With increasing nonlinearity, the vibrations for cases with $x_0 = -0.5$ eventually become essentially chaotic. There appears to be a threshold level of vibration amplitude, which is not well defined but above which chaotic vibrations occur. The initial amplitudes of vibration can be increased by imagining a situation where the vortex is created closer to the plate. Figure 4 shows calculated results for $x_0 = 0.5$, i.e., the vortex is inserted above the plate center. Note that

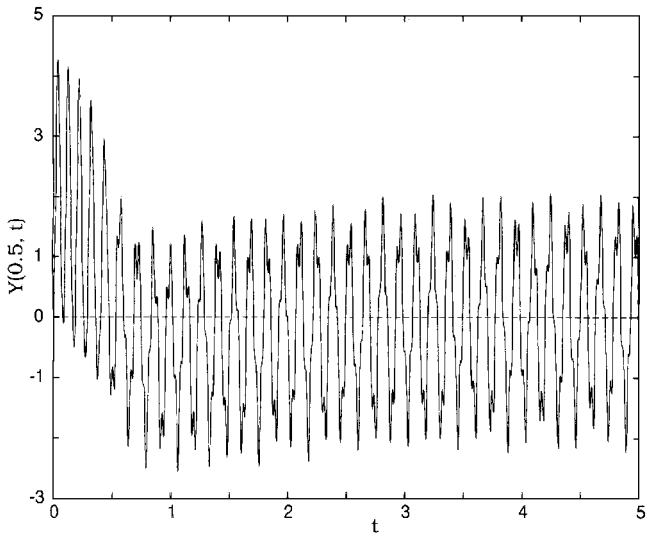

a) $\varepsilon = 100$

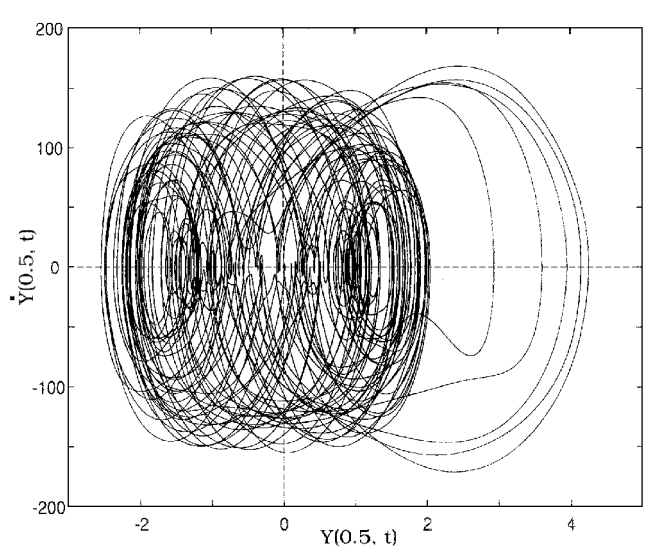

b) Phase plane trajectories for $\varepsilon = 100$

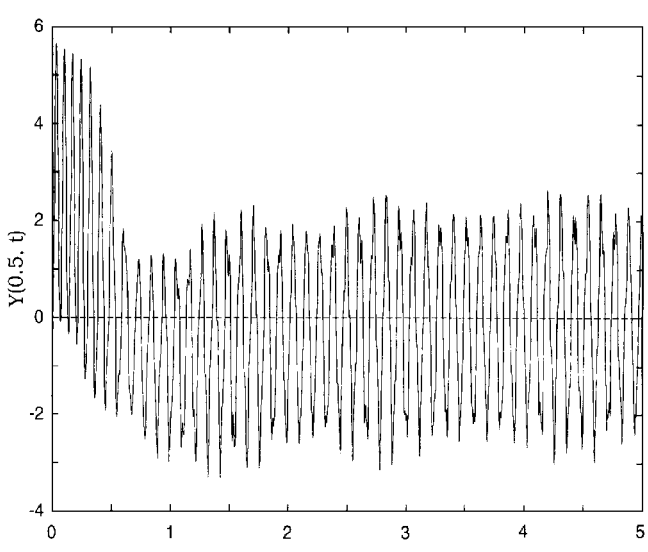

c) $\varepsilon = 500$

Fig. 4 Vibrations induced for $x_0 = 0.5$.

more complex vibrations now occur. As shown in Fig. 4b, relatively high velocities are achieved, and the phase plane trajectories are essentially chaotic. An implication of the results shown in Figs. 3 and 4, as well as other computations, is that once a disturbance induces a plate oscillation of a certain threshold amplitude, then irregular and chaotic vibrations will occur. This threshold is difficult to determine precisely, but is believed to be somewhere around 1.75–2 times the plate thickness. It is not possible here to define an objective criterion for the boundary between regular (but perhaps complicated) vibrations and the irregular patterns that are observed at larger values of ε. For example, the case shown in Fig. 3b is believed to be close to the threshold and does exhibit some minor tendencies toward irregularity; however, the irregularity is nowhere as pronounced as in Fig. 4a where the initial pressure field generates a vibration of larger amplitude.

The interaction described thus far is between the inviscid external flow and the plate. However, this is not the only type of interaction that must be considered. It is well known that a convected vortex above a solid surface can provoke boundary-layer separation in a variety of circumstances depending on the value of the fractional convection rate α (Refs. 3 and 6). In addition, it is known that a boundary layer on a moving surface can also separate.[17] At high Reynolds numbers, the process of boundary-layer separation is very complex[3–5] and difficult to compute accurately. The process generally initiates within the boundary layer in a region where the external pressure gradient is adverse. Separation is usually preceded by the appearance of a zone of recirculation, and shortly thereafter a sharp streamwise focusing of boundary-layer vorticity occurs abruptly, leading to the ejection of a narrow plume of concentrated vorticity. Usually, the net result of this process is the creation of a new vortex as the ejected boundary-layer plume rolls up into a vortex in a strong inviscid–viscous interaction with the external flow. To date such phenomena have been clearly observed in experiments,[3] but it has only been possible to calculate the onset of the interactive event.[6] What is known concerning such phenomena is that sharp local pressure spikes can occur, and these have the potential to provoke further motion of the plate.

Rather than attempt to calculate the complicated evolving boundary-layer flow on the moving plate, a simulation of the pressure spike at separation was introduced into the present calculations. In general, the time until separation for a given fractional convection rate depends on the length of time the boundary layer has been exposed to the vortex.[3,16] Here, however, the pressure spike was arbitrarily assumed to occur at $x = 0.5$ when the vortex was directly above the plate center. The assumed spike perturbation pressure was

$$p_s = -(c_1\bar{x} + c_2)\, e^{-\bar{x}^2/c_3^2} \tag{43}$$

and this was superimposed on Eq. (42) instantaneously when the vortex center was at $x = 0.5$. For the cases reported here, $c_1 = 300$, $c_2 = 6$, and $c_3 = 0.04$, which yield a narrow spatial spike. Because the separation event is a localized transient, the disturbance (43) was maintained for an arbitrary period of 0.1 time unit. The imposed pressure with spike is shown in Fig. 5, and it may be verified that this distribution is similar to that calculated for a separating boundary layer.[6]

Representative results for this case are shown in Fig. 6. Evidently the model separation pressure spike pushes the deflection over the threshold amplitude for $\varepsilon = 500$ (cf. Fig. 3b) and an irregular chaotic vibration of the plate ensues. The phase plane trajectories for these vibrations appear chaotic, similar to that shown in Fig. 4b.

VI. Nonlinear Resonance

In this section, the nature of the oscillations produced when the system is forced by a convective pressure wave of the form

$$p = P_0 \sin\left(\tilde{\alpha}x - \gamma_1^2 t\right) \tag{44}$$

is considered. Here $\tilde{\alpha}$ is a scaled convection velocity whose particular value has a minor effect on the results to be shown here, which are for $\tilde{\alpha} = 1.0$. The forcing pressure described by Eq. (44) could be due to oscillations of an upstream control surface or due to a convected

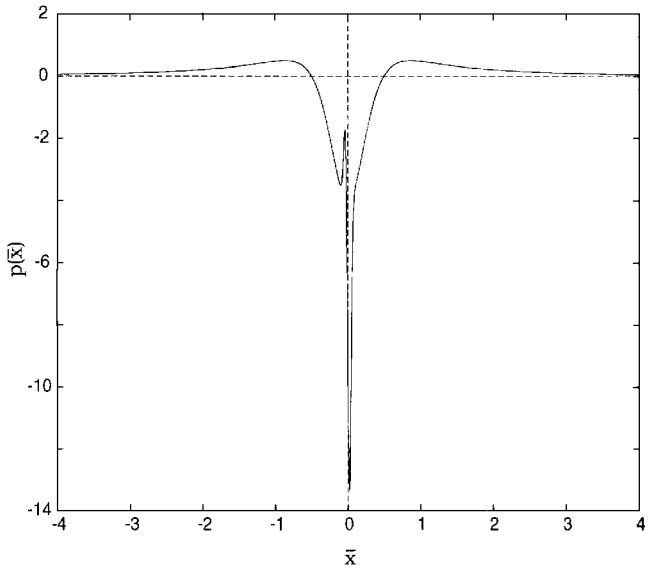

Fig. 5 Instantaneous induced pressure distribution due to a convected vortex and a model boundary-layer separation event.

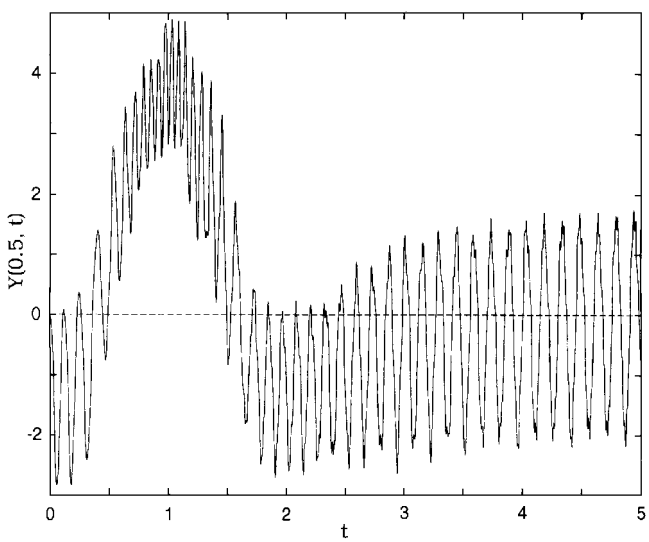

Fig. 6 Centerpoint deflection for $x_0 = -0.5$ with a model pressure spike introduced at $t = 1$ for $\varepsilon = 500$.

array of vortices shed from some airframe feature upstream. The latter situation could be modeled as a vortex street, but the pressure field described by Eq. (44) is much simpler and, at the least, representative of such situations. The amplitude of the pressure wave is P_0, and in normal circumstances a deflection $O(P_0/\gamma_1^4)$ is anticipated; thus, take $\eta_m = P_0/\gamma_1^4$ in Eq. (19). Calculations were initiated at $t = 0$ when it was assumed that $\eta(x, 0) = \dot{\eta}(x, 0) = 0$. When $\varepsilon = 0$ in Eq. (19) and the plate is forced at the natural frequency γ_1^2 [as in Eq. (44)], a phenomenon of resonance and unbounded growth in the oscillation, which is linear in t, is expected. This behavior is shown in Fig 7a.

The same calculation for $\varepsilon = 0.002$ is shown in Fig. 7b, with the phase plane trajectories in Fig. 7c. It may be observed that the effect of the nonlinearity is to limit the unbounded growth of the linear case and at the same time to produce a rather complex limit cycle with beating. As ε increases, the vibration becomes progressively more complex, as shown in Figs. 7d–7f for $\varepsilon = 0.01$ and 2. It soon becomes no longer possible to identify a repeatable limit cycle behavior, and the clear trend is to higher frequency oscillations and almost chaotic behavior. Note that the maximum amplitude of the oscillation increases as ε increases and that the oscillations shown in Fig. 7f, for example, are over a range that is several times the plate thickness.

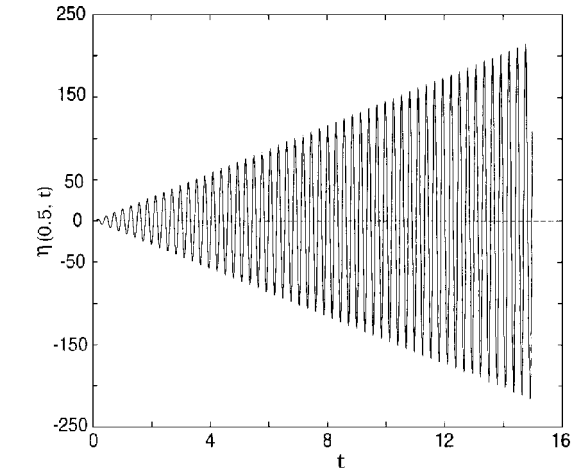

a) $\varepsilon = 0$

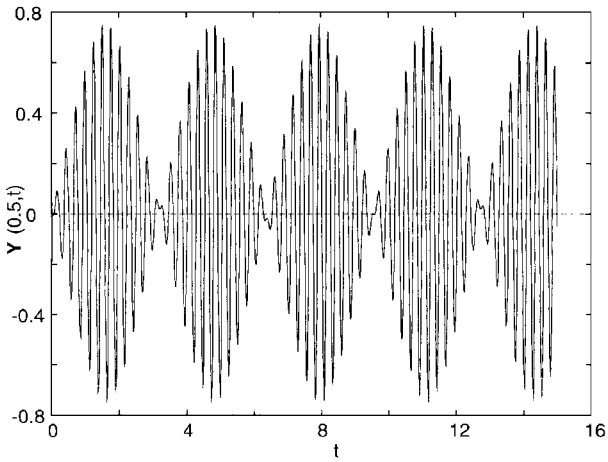

d) $\varepsilon = 0.001$

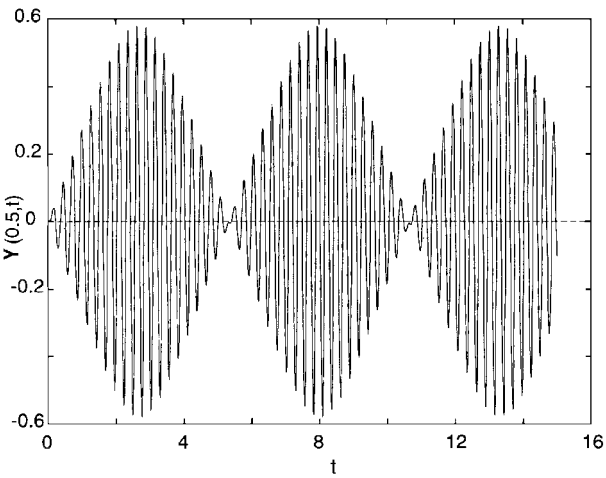

b) $\varepsilon = 0.002$

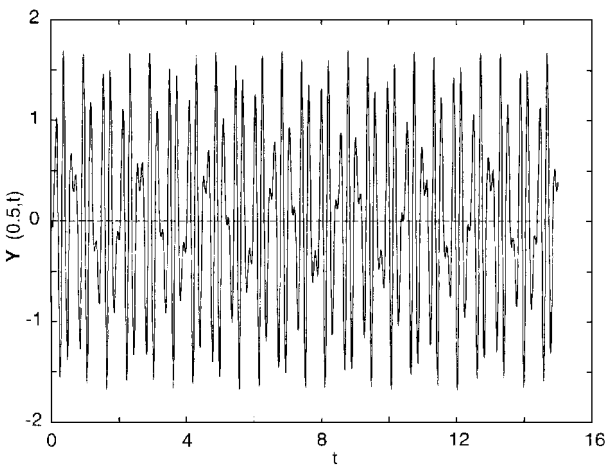

e) $\varepsilon = 2.0$

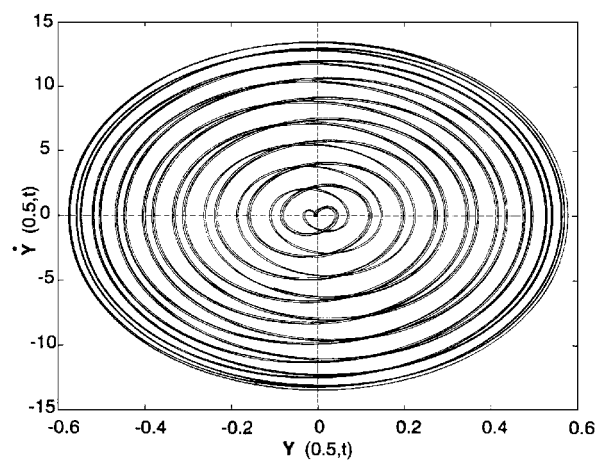

c) $\varepsilon = 0.002$

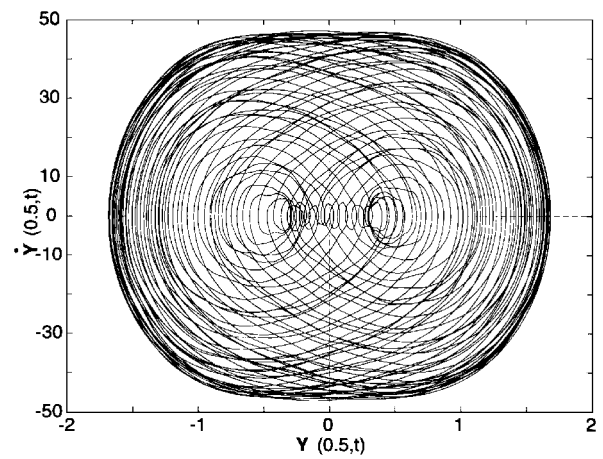

f) $\varepsilon = 2.0$

Fig. 7 Oscillations for resonance due to a convected pressure wave.

VII. Conclusions

The possible vibrational modes of a two-dimensional plate forced by various types of disturbances have been considered. Note that, whereas specific initial conditions such as Eq. (32) were employed to produce the graphs shown here, calculations were also carried out for a wide range of other initial conditions, and much the same results were found. It has been found that nonlinear effects play an important role in the plate dynamics. Increasing nonlinearity in the system generally acts to excite higher modes of vibration and has the overall effect of increasing the frequency of the plate oscillation. For relatively small values of ε [the coefficient of the nonlinear term in Eq. (19)], the oscillations are complex but generally are not limit cycles. On the other hand, once the disturbance that provokes the oscillation is sufficiently strong to induce amplitudes above a threshold value, essentially chaotic oscillations are provoked. The threshold value is difficult to determine precisely but appears to be from 1.75 to 2 times the plate thickness. In fact, the boundary between irregular but complex behavior and chaotic motion is difficult to determine precisely. Calculations were carried out to evaluate the Fourier transform of the centerpoint deflection $Y(t)$. For weakly nonlinear cases,

the computed spectrum showed one or more discrete frequencies, as expected. However, for the highly nonlinear cases, e.g., Figs. 2e and 4c, the spectrum shows a number of frequencies where a maximum occurs, with an almost continuous range of frequencies excited nearby; these ranges broaden appreciably as the length of the time record is increased suggesting a transition to chaotic behavior.

In the airframe environment, stimuli for initiation of plate motion may come from a variety of sources, including those of the pressure field due to a convected vortex, a convected pressure wave (a vortex train), or the boundary-layer separation that has been considered here. In general, the overall surface motion involves a complex interaction between the moving surface, the viscous boundary layer, and the external flowfield. The present work gives an indication of how complex the vibrational pattern can become; for three-dimensional plates further complexities can be expected because of the extra degree of freedom in possible plate vibrations and the complex nature of boundary-layer separation in three dimensions.[3] Note, however, that most of the vibrational patterns studied are not limit cycles; rather they are complicated motions that do not exactly repeat themselves with time and that at sufficiently large amplitude become chaotic. At the same time, some of the motions studied might appear, at first glance, to be of the limit cycle type, when observed in a practical situation. Last, the present theory does not account for structural damping, and future work will determine whether this has a major effect on the conclusions of the study.

Acknowledgments

This work was supported by the Air Force Office of Scientific Research under Grants F49620-93-1-1034 and F49620-96-1-10255. The authors would like to acknowledge several useful technical discussions with E. Varley and K. Zalutsky.

References

[1]Cunningham, A. M., Jr., "Practical Problems: Airplanes," *Unsteady Transonic Aerodynamics*, edited by D. Nixon, Vol. 120, Progress in Astronautics and Aeronautics, AIAA, Washington, DC, 1989, pp. 75–132.

[2]Mabey, D. G., "Physical Phenomena Associated with Aerodynamic Flows," *Unsteady Transonic Aerodynamics*, edited by D. Nixon, Vol. 120, Progress in Astronautics and Aeronautics, AIAA, Washington, DC, 1989, pp. 1–58.

[3]Doligalski, T. L., Smith, C. R., and Walker, J. D. A., "Vortex Interactions with Walls," *Annual Review of Fluid Mechanics*, Vol. 26, 1994, pp. 573–616.

[4]Cowley, S. J., Van Dommelen, L. L., and Lam, S. T., "On the Use of Lagrangian Variables in Description of Unsteady Boundary-Layer Separation," *Philosophical Transactions of the Royal Society of London*, Vol. 333, 1991, pp. 343–378.

[5]Peridier, V. J., Smith, F. T., and Walker, J. D. A., "Vortex-Induced Boundary-Layer Separation. Part 1. The Unsteady Limit Problem $Re \rightarrow \infty$," *Journal of Fluid Mechanics*, Vol. 232, 1991, pp. 99–131.

[6]Peridier, V. J., Smith, F. T., and Walker, J. D. A., "Vortex-Induced Boundary-Layer Separation. Part 2. Unsteady Interacting Boundary-Layer Theory," *Journal of Fluid Mechanics*, Vol. 232, 1991, pp. 133–165.

[7]Dowell, E. H., "Nonlinear Oscillations of a Fluttering Plate," *AIAA Journal*, Vol. 4, No. 7, 1966, pp. 1267–1275.

[8]Dowell, E. H., *Aeroelasticity of Plates and Shells*, Noordhoff International, Leyden, The Netherlands, 1975, Chap. 3.

[9]Holmes, P. J., "Bifurcations to Divergence and Flutter in Flow-Induced Vibrations: A Finite Dimensional Analysis," *Journal of Sound and Vibration*, Vol. 53, 1977, pp. 471–503.

[10]Holmes, P. J., "Nonlinear Dynamics, Chaos and Mechanics," *Applied Mechanics Review*, Vol. 43, 1990, pp. 823–838.

[11]Holmes, P. J., and Marsden, J., "A Partial Differential Equation with Infinitely Many Periodic Orbits: Chaotic Oscillations of a Forced Beam," *Archive for Rational Mechanics and Analysis*, Vol. 76, 1981, pp. 135–166.

[12]Love, A. E. H., *A Treatise on the Mathematical Theory of Elasticity*, 4th ed., Dover, New York, 1944, pp. 557–568.

[13]Press, W. H., Teukolsky, S. A., Vetterling, W. T., and Flannery, B. P., *Numerical Recipes*, 2nd ed., Cambridge Univ. Press, New York, 1992, Chap. 16.

[14]Kevorkian, J., and Cole, J. D., *Perturbation Methods in Applied Mathematics*, Springer–Verlag, Berlin, 1980, Chap. 3.

[15]Filon, L. N. G., *Proceedings of the Royal Society of Edinburgh*, Vol. 49, 1929, pp. 38-47.

[16]Doligalski, T. L., and Walker, J. D. A., "The Boundary Layer Due to a Convected Two-Dimensional Vortex," *Journal of Fluid Mechanics*, Vol. 139, 1984, pp. 1–28.

[17]Kiran, A. S., Varley, E., and Walker, J. D. A., "Unsteady Motion Induced on a Flexible Surface in a High Reynolds Number Flow," AIAA Paper 96-2138, June 1996.